

Stress interactions between two asymmetric noncircular tunnels

You-Sung La^a, Bumjoo Kim^{*}, Yeon-Soo Jang^b and Won-Hyuk Choi^c

Department of Civil and Environmental Engineering, Dongguk University, 30, Pildong-ro 1-gil, Jung-gu, Seoul, Republic of Korea

(Received June 3, 2017, Revised February 8, 2018, Accepted March 23, 2018)

Abstract. The continually growing demand for underground space in dense urban cities is also driving the demand for underground highways. Building the underground highway tunnel, however, can involve complex design and construction considerations, particularly when there exists divergence or convergence in the tunnel. In this study, interaction between two asymmetric noncircular tunnels—that is, a larger main tunnel and a smaller tunnel diverging from the main tunnel, was investigated by examining the distributions of the principal stresses and the strength/stress ratio for varying geometric conditions between the two tunnels depending on diverging conditions using both numerical analysis and scale model test. The results of numerical analysis indicated that for the 0°, 30°, 60° diverging directions, the major principal stress showed an initial gradual decrease and then a little steeper increase with the increased distance from the left main tunnel, except for 90° where a continuous drop occurred, whereas the minor principal stress exhibited an opposite trend with the major principal stresses. The strength/stress ratio showed generally a bell-shaped but little skewed to left distribution over the distance increased from the left larger tunnel, similarly to the variation of the minor principal stress. For the inter-tunnel distance less than 0.5D, the lowest strength/stress ratio values were shown to be below 1.0 for all diverging directions (0°, 30°, 60° and 90°). The failure patterns observed from the model test were found to be reasonably consistent with the results of numerical analysis.

Keywords: underground highway; noncircular tunnel; principal stress; diverging condition; strength-stress ratio

1. Introduction

With increasing interests on deep urban underground roads as the solution to the problems of traffic congestion, lack of above-ground space, and environmental pollution, the construction of underground expressways has been receiving considerable attentions in Korea. As for the types of underground expressway tunnel, a double-deck tunnel may be a fascinating alternative to two parallel tunnels due to the lower construction cost. However, since the underground expressway should have ramp tunnels connecting surface level to main tunnel deep underground, the double-deck tunnel can involve more complicated construction processes, especially for the section where the tunnel is diverged or converged, compared with two parallel tunnels. For instance, when a 1-level ramp tunnel is diverged from the 2-level main double-deck tunnel, the geometric conditions between the two tunnels in the divergence section become relatively complicated, which may make the interaction between the two tunnels more complex, giving rise to instability problems.

Interaction between adjacent tunnels have been studied by many researchers (Ghaboussi and Ranken 1977, Xie *et al.* 2004, Gerçek 2005, Chegade and Shahrour 2008, Kim and Bae 2008, Hsiao *et al.* 2009, Kim *et al.* 2012, Chung *et*

al. 2013, Kim and Lee 2013, Lee *et al.* 2013, Kang *et al.* 2014, Jung *et al.* 2014, Do *et al.* 2014, Lim and Son 2014, Nawel and Salah 2015, Das *et al.* 2017, Zheng *et al.* 2017, Kim and Kim 2017). Ghaboussi and Ranken (1977) performed a series of two-dimensional finite element analyses to study the behavior of a system of two parallel and adjacent tunnels by considering various sequences of excavation. The ground was modelled as an elastic material. The results indicated that, for the configurations investigated, the computed interactions between two parallel tunnels were small when the centre-line spacing was greater than about two tunnel diameters. Xie *et al.* (2004) studied the stability of two parallel circular tunnels with different diameters in cohesive soil by investigating the relationship between the collapse stability ratio and the pillar width between the two tunnels using finite element method (FEM). They reported that the pillar width had a critical value of 18m when the diameter ratio of two parallel circular tunnels was 2 and the thickness of the cover soil was equal to the diameter of the larger tunnel, and further increase in the pillar width would not result in a significant increase in the collapse stability ratio. Chegade and Shahrour (2008) performed a parametric study on twin circular tunnels using FEM to examine the effect of the relative position of tunnels (i.e., aligned-horizontally, vertically and inclined between the twin tunnels) and the construction procedure on soil movement and internal forces in the lining. They reported that the highest soil settlement is obtained for vertical aligned tunnels, while horizontal aligned tunnels cause the lowest settlement. Do *et al.* (2014) performed a numerical investigation on the influences of the segment joints and tunnel distance on the

*Corresponding author, Professor
E-mail: bkim1@dongguk.edu

^aPh.D. Student

^bProfessor

^cGraduate Student

structural lining forces induced in twin tunnels and reported that the structural lining forces induced in the first tunnel through various phases are considerably affected by the second tunnel construction process. Kang *et al.* (2014) studied the behavior of rock pillar in the diverging area of road tunnel by a three-dimensional numerical simulation and proposed a safety factor chart to reflect the effects of pillar width, tunnel overburden depth, and rock condition. They found that the safety factors show nonlinear distributions with respect to overburden depth and rock class with increasing the pillar width. Nawel and Salah (2015) also studied numerically the interaction effects caused by the construction of two parallel tunnels by considering several parameters such as tunnel size, depth, the relative position between two tunnels and lining thickness. On the other hand, Kim and Bae (2008) performed a series of scaled model test on three parallel tunnels and investigated their stability by examining crack initiating pressures and deformation behaviors. The results showed that shallower pillar widths are unstable because of lower crack initiating pressures and larger tunnel convergences compared with thicker pillar widths. Lee *et al.* (2013) investigated the behaviors of two parallel tunnels subjected to different types of enlargement using FEM and reported that for the tunnels with the same pillar width after enlarged, uni-lateral enlargement induced higher deformations compared with the bi-lateral enlargement.

Concerning the interaction between adjacent tunnels, however, most studies have been focused on parallel tunnels as described and, moreover, many cases of which were for circular tunnels or for tunnels in symmetric conditions. Little attention has been paid to the interaction between two tunnels in asymmetric geometric configurations. This study concerns the interaction between two asymmetric noncircular tunnels. Specifically, interactions between a large-diameter double-deck tunnel and a ramp tunnel with smaller diameter diverging right from upper level of the main double-deck tunnel, all constructed using New Austrian Tunneling Method (NATM), are considered. In order to investigate the interactions between the two tunnels, a numerical analysis was performed using 2-D finite difference method (FDM), and the stresses between two tunnels in various geometric configurations were analyzed. The tunnel stability and the effect of geometric conditions were examined by calculating strength-stress ratio between the two tunnels. Model tests were also carried out on some of the geometric configurations used in the numerical analysis to examine further interaction behavior between two tunnels and to compare with the results of the analysis.

2. Methods

2.1 Numerical analysis

Since the case employed in this study was about two NATM tunnels-that is, a main double-deck tunnel and a ramp tunnel diverging right from upper level of the main 2-level tunnel, various geometric conditions between the main- and the diverging tunnel depending on varying

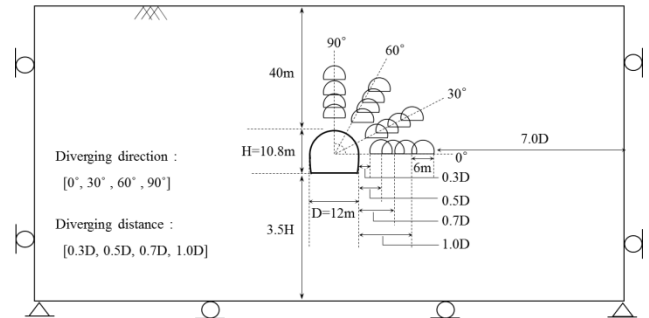


Fig. 1 Cross-section for numerical analysis adopted in this study

Table 1 Rock mass properties used in analysis

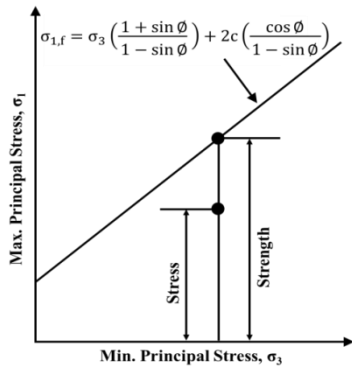
Rock mass	Unit weight (kN/m ³)	Elastic Modulus (MPa)	Cohesion (kPa)	Friction angle (°)	Poisson ratio (ν)
RMR class V	23	580	170	34	0.26

diverging distances and diverging directions were considered for a numerical analysis. The term ‘diverging distance’ was here used to mean inter-tunnel distance - that is, the distance separated between the main tunnel and the diverging tunnel. As for the main tunnel, one-way, two-lane double-deck tunnel with 12 m in width and 10.8 m in height was assumed to be located at 40 m deep underground rock mass. For the diverging tunnel, one-lane tunnel with 6m in width and 4m in height was adopted and assumed to be diverged from upper level of the main double-deck tunnel. For this case, the numerical analysis was performed on a total of sixteen different geometric conditions between the two tunnels by considering four diverging distances (i.e., 0.3D, 0.5D, 0.7D and 1.0D; separated distance between the main tunnel and each diverging tunnel, D = the largest width of the cross-section of the main tunnel) and four diverging directions (i.e., 0°, 30°, 60°, and 90°; angle between horizontal direction and diverging tunnel direction from the center of the main tunnel cross-section). Fig. 1 represents the sketch of the 2-D analysis cross-section in which all the diverging conditions analyzed are displayed together.

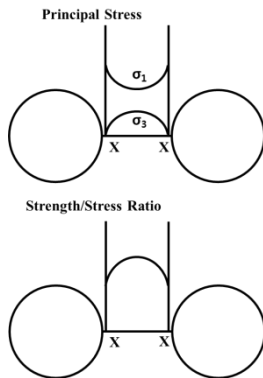
The main tunnel and the diverging tunnels were all assumed to be excavated in the same ground condition - that is, in an RMR class IV rock mass with the ratio of horizontal stress to vertical stress of 1.0. The ground rock mass was modeled using Mohr-Coulomb and elastic parameters and FLAC 2D (version 6.0) software employing finite difference approach was used for this numerical analysis. The model parameters used in the analysis is shown in Table 1.

Interaction between the main tunnel and the diverging tunnel for the varying diverging conditions using the numerical analysis was investigated upon when the diverging tunnel adjacent to pre-existing main tunnel is excavated in full face by examining major and minor principal stresses (σ_1 and σ_3) between the two tunnels.

Hoek and Brown (1980) proposed the following empirical relationship between the principal stresses for intact rock at failure based on classical Griffith crack theory for plane compression and the analysis of a wide range of



(a) Mohr-Coulomb strength criterion in terms of σ_1 and σ_3



(b) σ_1 and σ_3 distributions and SSR between two parallel circular tunnel

Fig. 2 Method and concept employed in this study

experimental data.

$$\frac{\sigma_{1,f}}{\sigma_c} = \frac{\sigma_3}{\sigma_c} + \sqrt{m \frac{\sigma_3}{\sigma_c} + s} \quad (1)$$

in which $\sigma_{1,f}$ = the major principal stress at failure; σ_3 = the minor principal stress; σ_c = the uniaxial compressive strength for the intact rock material; and m and s = constants that depend on the properties of the rock and on the extent to which it had been broken before being subjected to the failure stresses $\sigma_{1,f}$ and σ_3 . On the other hand, Mohr-Coulomb failure criterion can be expressed in terms of the major and minor principal stresses at failure as follows

$$\sigma_{1,f} = \sigma_3 \left(\frac{1 + \sin \phi}{1 - \sin \phi} \right) + 2c \left(\frac{\cos \phi}{1 - \sin \phi} \right) \quad (2)$$

where, c = cohesive strength; ϕ = angle of friction. Equivalent angle of friction and cohesive strength for each rock and stress range can be determined by fitting Eq. (2) showing the linear relationship between $\sigma_{1,f}$ and σ_3 to the curve generated by solving Eq. (1). For rock masses, the equivalent Mohr-Coulomb parameters can also be determined in the same way as for intact rock by using the generalized Hoek-Brown failure criterion applicable to rock masses (Hoek and Brown, 1997) instead of using the failure criterion for intact rock (Eq. (1)). In this analysis, therefore, the strength of rock mass was determined by using the equivalent Mohr-Coulomb parameters (i.e., c and ϕ) shown in Table 1. For an given (induced) σ_3 , the induced σ_1 was

then compared with the rock mass strength $\sigma_{1,f}$ to obtain the Strength/Stress Ratio (SSR) defined by

$$SSR = \frac{\sigma_{1,f}}{\sigma_1 | \sigma_3} \quad (3)$$

Fig. 2 represents the Mohr-Coulomb strength criterion expressed in terms of principal stresses and the concept of SSR.

For a detail examination, the magnitude and the distribution of principal stresses and the SSR were obtained for three sectional areas between the two tunnels for each geometric condition, as shown in Fig. 3.

2.2 Laboratory scale model test

The effect of different geometric conditions between the two asymmetric noncircular tunnels (i.e., main- and diverging tunnels in different diverging conditions) on the stability of tunnels was also examined by performing laboratory scale model tests and observing failures occurred in model tunnels. Tunnels at 1:100 scale were used in this test. As shown in Fig. 4, the scale model equipment

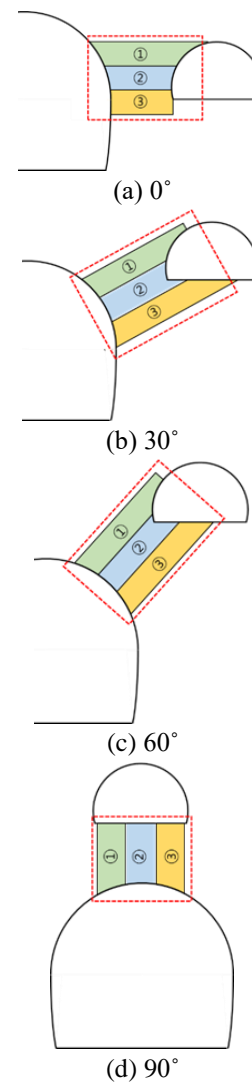
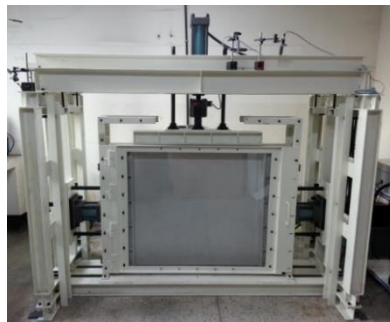
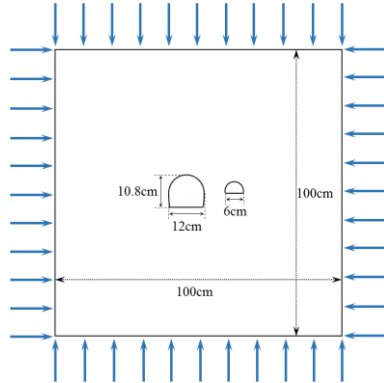


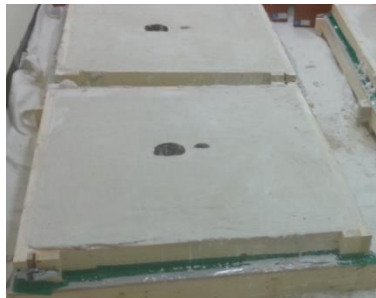
Fig. 3 Diverging direction and three sectional inter-tunnel zones



(a) Scale model test equipment



(b) Model size and test condition



(c) Rock mass specimen



(d) Model tunnels

Fig. 4 Tunnel model test set-up

is composed of an outside steel frame of about 2.5 m in length and 2.0 m in height, an inside steel box frame to hold a specimen with the size of 1.0 m length \times 1.0 m height \times 0.1 m thickness, servo motor actuator and three 10-ton capacity rams mounted on the outside frame used to push the inside steel frame in three different directions; top to down, left to right and right to left, respectively. The front and back sides of the inside frame are covered with a transparent, tempered acrylic panel and a steel plate, respectively, so that the specimen can be loaded in a plane strain condition as the inside frame constrains it while visual observation of the

Table 2 Similarity ratio in the scale model system

Type	Parameters	Dimension	Similarity ratio
Geometry	Length, L	L	$1/10^2$
	Rotation, θ	-	1
	Strain, ϵ	-	1
	Area, A	L^2	$1/10^4$
Material	Elastic modulus, E	FL^{-2}	$1/144$
	Poisson ratio, ν	-	1
	Density, ρ	FT^2L^{-4}	$1/1.44$

specimen through the front side panel becomes available during the test. The test is computer-controlled, and the load-displacement histories are recorded automatically. In this study, the loading was applied by controlling the constant displacement rate of 2 mm per minute. A Nikon high-performance digital camera was used to capture fractures occurred in the specimen during loading.

A rock mass specimen (i.e., scale model rock mass) with the size of 1.0 m (height) \times 1.0 m (width) \times 0.1 m (thickness) was prepared first by mixing Jumunjin sand, gypsum, and water with the mixture ratio of 52%, 15% and 33% in weight, respectively. Since the sizes of model tunnels were to be reduced to 1/100 of the original sizes, the model rock mass needed to be made to have the material parameters scaled down in accordance with the similarity law as shown in Table 2. The sand-gypsum-water mixture ratio used in the preparation of the rock mass specimen was hence determined by performing unconfined compressive strength tests for sand-gypsum-water mixture samples with various mixture ratio. The corresponding unconfined compressive strength was found to be 0.313 MPa at 28 days. Accordingly, following the completion of mixing, each mixture was poured into a wooden frame, whose inside dimensions are equal to that of the rock mass specimen, and cured for 28 days until the test. Model tunnels were prepared by placing two steel frames with the same size and shape as the model tunnels at predetermined locations inside the wooden frame prior to pouring the mixture. Both the tunnel shaped-steel frames and the mixture material cured inside the steel frames were removed together right before the test. The tunnel model test was conducted on four different geometric conditions—that is, with three different diverging directions of 0° , 30° , 60° at the diverging distance of $0.3D$ and the diverging angles of 90° at the diverging distance of $1.0D$.

3. Results

3.1 Numerical analysis results

3.1.1 Distribution of principal stresses between two tunnels

Fig. 5 represents the distribution of the major and minor principal stresses (σ_1 and σ_3) induced in the middle area of the three sectional areas (i.e., zone 2 shown in Fig. 3) between the two tunnels for the sixteen different geometric conditions—that is, four diverging distances for four

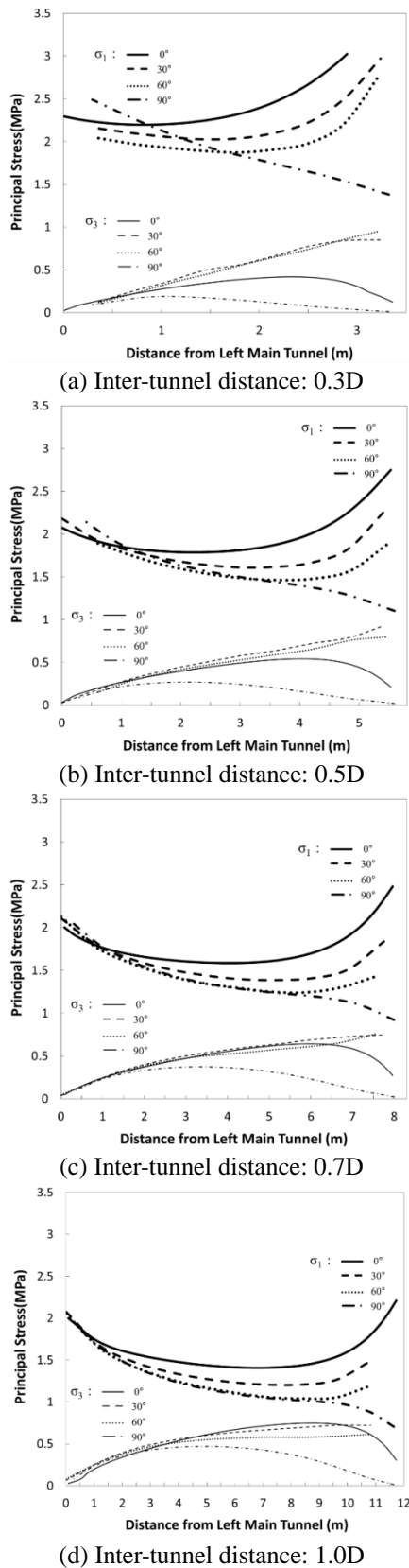


Fig. 5 Distribution of major and minor principal stresses

diverging directions, depending on the diverging conditions of the smaller right directional ramp tunnel (i.e., inter-tunnel distances of 0.3D, 0.5D, 0.7D and 1.0D for the

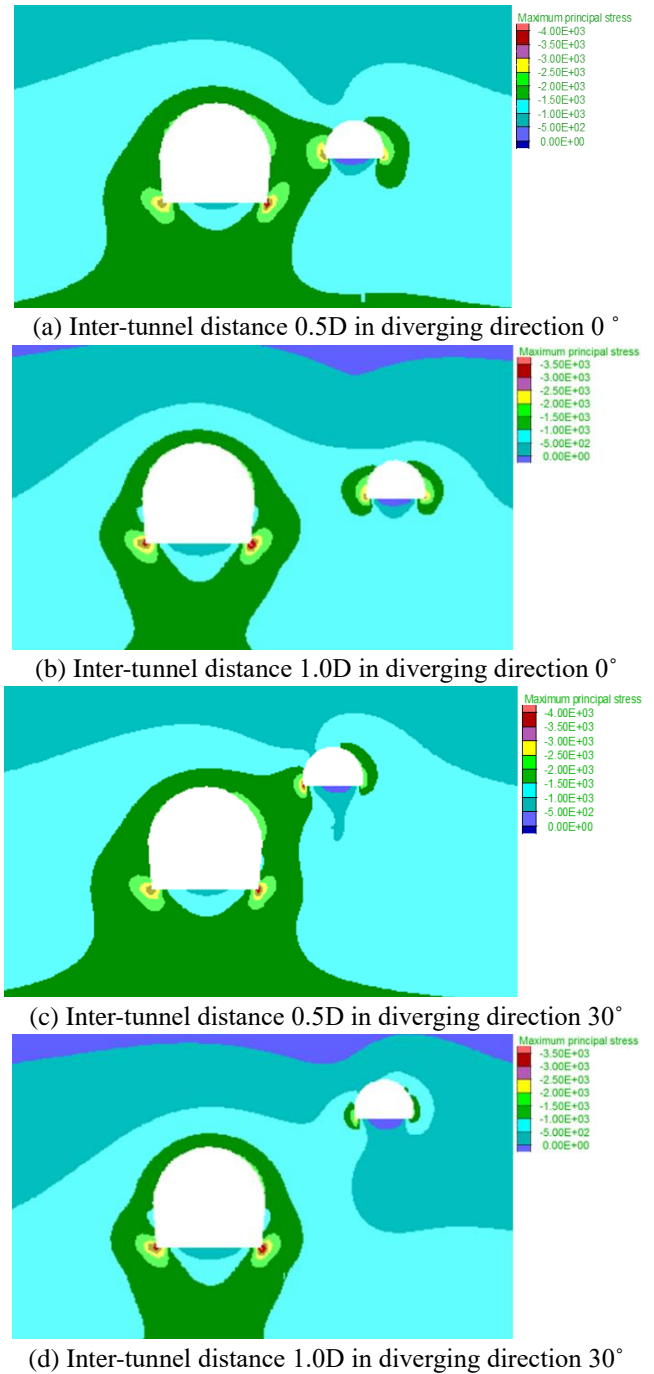


Fig. 6 Major principal stress contour

diverging directions of 0°, 30°, 60° and 90° between the two tunnels).

The results indicated that the overall trend in the distributions of both σ_1 and σ_3 with varying the diverging distance is similar between the same diverging directions. Except for the case of 90° diverging direction, the σ_1 showed an initial gradual decrease near the larger main tunnel and then a little steeper increase, as the distance from the main tunnel (left) is increased further and becomes close to the smaller diverging tunnel (right). For the three diverging directions (i.e., 0°, 30°, 60°), the highest σ_1 was all induced around the diverging tunnel and was reduced with the increased diverging direction angle from 0° to 60°.

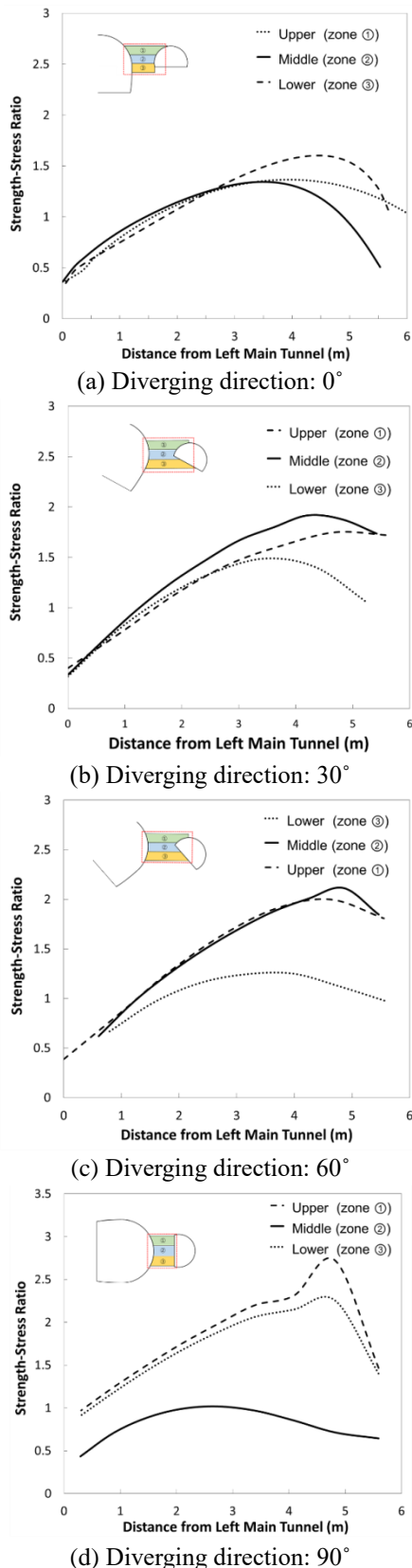


Fig. 7 Strength/Stress Ratio (SSR) for Inter-tunnel distance 0.5D

For the case of 90° diverging direction, however, a continuous drop in σ_1 occurred with increasing the distance from the main tunnel. In contrast to the distribution of the

σ_1 , the σ_3 showed an initial gradual rise near the left main tunnel and then a little steeper reduction with increasing the distance from the left main tunnel for both 0° and 90° diverging direction cases, whereas for 30° and 60° cases it showed a continuous increase and a subsequent plateau phase. As the diverging distance (i.e., separated distance between the two tunnels) increased from 0.3D to 1.0D, the magnitudes of σ_1 , generally became smaller.

Fig. 6 displays the contours of the σ_1 induced between the two tunnels separated by 0.5D and 1.0D for 0° and 30° diverging direction conditions, respectively. It is seen that besides the largest stresses occurred around the invert corners, relatively high stresses are induced at the middle of inter-tunnel distance for 0.5D case, compared with 1.0D.

3.1.2 Distribution of Strength/Stress Ratio between two tunnels

Fig. 7 shows the strength/stress ratio (SSR) obtained using Eq. (3) for four diverging directions at the diverging distance of 0.5D. Similarly to the variation of σ_3 in Fig. 5, the SSR showed generally a bell-shaped but little skewed to left distribution over the distance increased from the left larger tunnel. By definition, for a material the value of SSR less than 1.0 indicates that the material strength is exceeded by the stress in the material. The 0° diverging direction condition (i.e., horizontally separated condition) exhibited relatively low SSR values along whole inter-tunnel distance over all three sectional levels (i.e., divided into upper, middle, and lower zone), compared to other diverging directions. For 0° and 30° diverging directions, the SSR values were all less than 1.0 within around 2 m apart from the left main tunnel, while for 60° and 90° diverging directions, they were all less than 1.0 over entire inter-tunnel distance specifically at lower level (zone 3) and middle level (zone 2), respectively.

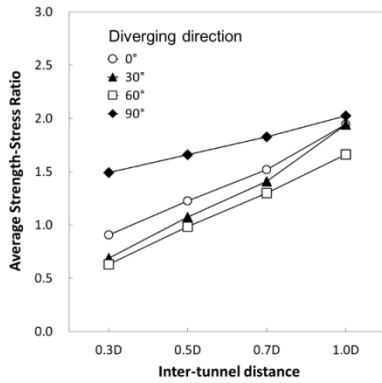
3.1.3 Relationship between Strength/Stress Ratio and diverging conditions

In Fig. 8(a)-8(c), the values of SSR averaged over inter-tunnel distance for each sectional zone (i.e., upper, middle, and lower) are shown with respect to sixteen different tunnel geometric conditions—that is, four diverging distance for four diverging direction conditions. It is obvious that the average SSR increases with the increased diverging distance, but the magnitudes of the ave. SSR show differences between the sectional zones as well as between the diverging directions. For the diverging distance larger than 0.5D, the ave. SSR values at upper zone were larger than 1.0 for all diverging directions except for 0° diverging case, whereas at lower zone the ave. SSR values larger than 1.0 for all diverging directions were obtained only at the diverging distance larger than 0.7D.

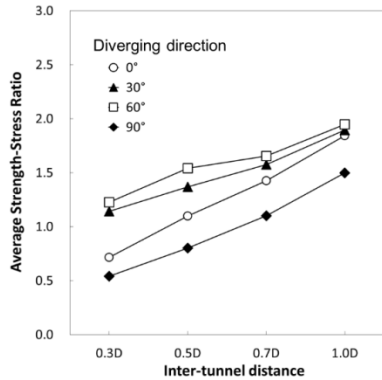
Fig. 8(d) represents the lowest ave. SSR values over the whole three zones for each diverging condition. It is seen that for all four diverging directions (0°, 30°, 60° and 90°), the lowest ave. SSR values are all below 1.0 when the diverging distance is less than 0.5D.

3.2 Model test results

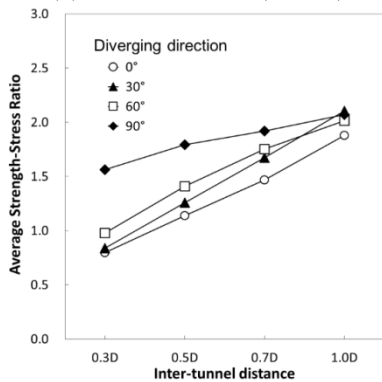
The four sets of two tunnels in four different geometric



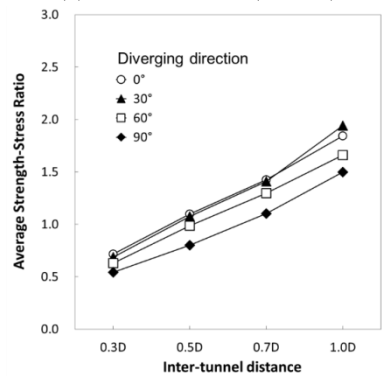
(a) At upper level (zone 1)



(b) At middle level (zone 2)



(c) At lower level (zone 3)



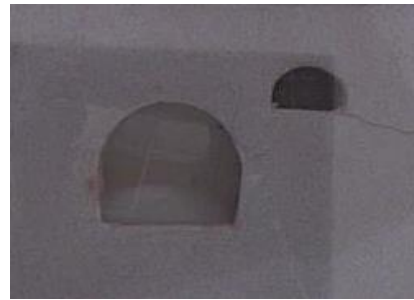
(d) The minimum over three levels

Fig. 8 Average SSR at different levels between the two tunnel

conditions—that is, 0°, 30°, 60° diverging directions at 0.3D diverging distance and 90° diverging direction at 1.0D diverging distance, were tested to examine their failure



(a) 0° diverging direction at 0.3D inter-tunnel distance



(b) 30° diverging direction at 0.3D inter-tunnel distance



(c) 60° diverging direction at 0.3D inter-tunnel distance



(d) 90° diverging direction at 1.0D inter-tunnel distance

Fig. 9 Model tunnels failed under loading

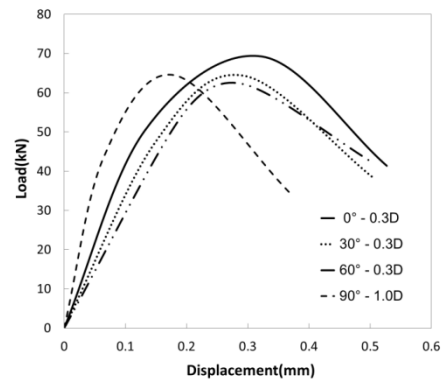


Fig. 10 Load-displacement behaviors during the test for four different diverging conditions

characteristics using scale models. Fig. 9 shows the model tunnels after the tests. For all the conditions, the failure occurred between the two tunnels. It was observed commonly that the inter-tunnel failure initiated at the boundary of each tunnel, with the first fracture in the left main tunnel, and propagated from the initiation points to inter-area along the diverging direction.

Fig. 10 displays the relationship between the load applied at the boundary of the specimen and the maximum displacement occurred in the inter-tunnel area, obtained from digital camera image analysis, during each test for the four diverging conditions. Similarly to the results of the numerical analysis, the load-displacement records indicated that the stability of the tunnels decreased slightly with increasing the diverging direction from 0°, 30° to 60° for a given inter-tunnel distance 0.3D.

Since the fractures occurred due to overstress, the failure patterns observed for these conditions may be understood by relating them to the distributions of stress and strength/stress ratio, if they are known. In this regard, the results of numerical analysis presented in 3.1.1 and 3.1.2 were found to be in a good agreement with these model test results.

4. Conclusions

In this study, interaction between two asymmetric noncircular tunnels (i.e., a larger main tunnel and a smaller tunnel diverging from the main tunnel) was investigated by examining the distributions of the principal stresses and the strength/stress ratio for varying geometric conditions between the two tunnels depending on diverging conditions using both numerical analysis and scale model tests.

The results of numerical analysis indicated that for the 0°, 30°, 60° diverging directions, the major principal stress shows an initial gradual decrease and then a little steeper increase with the increased distance from the left main tunnel, except for 90° where a continuous drop occurs, whereas the minor principal stress exhibits an opposite trend with the major principal stresses - that is, an initial gradual rise near the left main tunnel and a subsequent steeper reduction (0° and 90°) or plateau phase (30° and 60°). The strength/stress ratio showed generally a bell-shaped but little skewed to left distribution over the distance increased from the left larger tunnel, similarly to the variation of the minor principal stress. It was also found that for the inter-tunnel distance less than 0.5D, the lowest strength/stress ratio values are all below 1.0 for all diverging directions (0°, 30°, 60° and 90°). From the scale model tests, it was observed that the inter-tunnel failure initiated at the boundary of each tunnel, with the first fracture in the left main tunnel, and propagated from the initiation points to inter-area along the diverging direction, as could be expected from the numerical analysis results.

Acknowledgements

This research was supported by Development of Design and Construction Technology for Double Deck Tunnel in Great

Depth Underground Space (14SCIP-B088624-01) from Construction Technology Research Program funded by Ministry of Land, Infrastructure and Transport of Korean government.

References

- Chehade, F.H. and Shahrour, I. (2008), "Numerical analysis of the interaction between twin-tunnels: Influence of the relative position and construction procedure", *Tunn. Undergr. Sp. Technol.*, **23**(2), 210-214.
- Chung, J.S., Moon, I.K. and Yoo, C.H. (2013), "Behaviour characteristics of tunnel in the cavity ground by using scale model tests", *J. Kor. Geo-Environ. Soc.*, **14**(12), 61-69.
- Das, R., Singh, P.K., Kainthoal, A., Panthee, S. and Singh, T.N. (2017), "Numerical analysis of surface subsidence in asymmetric parallel highway tunnels", *J. Rock Mech. Geotech. Eng.*, **9**(1), 170-179.
- Do, N.A., Dias, D., Oreste, P. and Djeran-Maigre, I. (2014), "2D numerical investigations of twin tunnel interaction", *Geomech. Eng.*, **6**(3), 263-275
- Gerçek, H. (2005), "Interaction between parallel underground openings", *Proceedings of the 19th International Mining Congress and Fair of Turkey*, İzmir, Turkey, June.
- Ghaboussi, J. and Ranken, R.E. (1977), "Interaction between two parallel tunnels", *J. Numer. Anal. Meth. Geomech.*, **1**(1), 75-103.
- Hoek, E. and Brown, E.T. (1980), "Empirical strength criterion for rock masses", *J. Geotech. Eng.*, **106**(GT9), 1013-1035.
- Hoek, E. and Brown, E.T. (1997), "Practical estimates of rock mass strength", *J. Rock Mech. Min. Sci.*, **34**(8), 1165-1186.
- Hsiao, F.Y., Wang, C.L. and Chern, J.C. (2009), "Numerical simulation of rock deformation for support design in tunnel intersection area", *Tunn. Undergr. Sp. Technol.*, **24**(1), 14-21.
- Jung, M.C., Hwang, J.S., Kim, J.S., Kim, S.W. and Baek, S.C. (2014), "Influence of the existing cavern on the stability of adjacent tunnel excavation by small-scale model tests", *J. Kor. Geo-Environ. Soc.*, **15**(12), 117-128.
- Kang, J.G., Yang, H.S. and Jang, S.J. (2014), "Stability analysis of rock pillar in the diverging area of road tunnel", *J. Kor. Tunn. Undergr. Sp. Assoc.*, **24**(5), 344-353.
- Kim, J.H. and Kim, J.W. (2017), "Stability estimation of the pillar between twin tunnels considering various site conditions," *J. Kor. Tunn. Undergr. Sp. Assoc.*, **27**(2), 109-119.
- Kim, J.K. and Lee, S. (2013), "A study on the estimation of the behaviors by compression method of rock pillar between close parallel tunnels", *J. Kor. Geo-Environ. Soc.*, **29**(12), 87-94.
- Kim, J.W. and Bae, W.S. (2008), "A study for the stability investigation of three parallel tunnels using scaled model tests", *J. Kor. Tunn. Undergr. Sp. Assoc.*, **18**(4), 300-311.
- Kim, W.B., Yang, H.S. and Ha, T.H. (2012), "An assessment of rock pillar behavior in very near parallel tunnel", *J. Kor. Tunn. Undergr. Sp. Assoc.*, **22**(1), 60-68.
- Lee, M.H., Kim, B., Jang, Y.S., Yun, J.N. and Park, H.G. (2013), "Behavior and pillar stability of enlarged existing parallel tunnels", *J. Kor. Tunn. Undergr. Sp. Assoc.*, **15**(5), 537-546.
- Lim, H.M. and Son, K.R. (2014), "The stability analysis of near parallel tunnels pillar at multi-layered soil with shallow depth by numerical analysis", *J. Kor. Geo-Environ. Soc.*, **15**(1), 53-62.
- Nawel, B. and Salah, M. (2015), "Numerical modeling of two parallel tunnels interaction using three-dimensional finite elements method", *Geomech. Eng.*, **9**(6), 775-791
- Xie, J., Gunn, M.J. and Rahim, A. (2004), "Collapse analysis for two parallel circular tunnels with different diameters in soil", *Proceedings of the 9th International Symposium on Numerical*

Models in Geomechanics, NUMOG IX, Ottawa, Canada,
August.

Zheng, G., Du, Y., Cheng, X., Diao, Y., Deng, X. and Wang, F.
(2017), "Characteristics and prediction methods for tunnel
deformations induced by excavations", *Geomech. Eng.*, **12**(3),
455-467

CC